International Journal of Civil Engineering (IJCE)
ISSN (P): 2278-9987; ISSN (E): 2278-9995
Vol. 7, Issue 1, Dec – Jan 2018; 9-30

International Academy of Science, Engineering and Technology
Connecting Researchers; Nurturing Innovations

DYNAMIC ANALYSIS OF THE S-TYPE FLUID-CONVEYING STEEL PIPE FOR TSEN-WENG RESERVOIR USING FINITE ELEMENT METHOD

Jong-Shyong Wu[1], Ching-An Huang[2] & Huei-Jou Shaw[3]

[1,3]Professor, Department of Systems and Naval Mechatronic Engineering, National Cheng-Kung University, Tainan, Taiwan, Republic of China

[2]Graduate Student, Department of Systems and Naval Mechatronic Engineering, National Cheng-Kung University, Tainan, Taiwan, Republic of China

ABSTRACT

About seven years ago, the first author was invited to attend a meeting held by the "South Water Resources Bureau" to discuss the problem about cleaning sediments of the Jsen-Weng Reservoir located at Tainan, Taiwan. At that time, a suggestion to replace "the conventional sluice gate near free water surface" by "the siphon with its inlet near reservoir bottom" (cf. Figure. A1 in Appendix) was presented and approved by all the attendees. Five years later, about two years ago, the first author was invited again to attend a meeting to review the report for a project about the construction of a tunnel for cleaning sediments of the Jsen-Weng Reservoir. The key point is to review the design of a "S-type water-conveying steel pipe" (or simply called "S-pipe") with its outlet connecting with an 1.2 km tunnel passing through a mountain. The pipe diameter is 10m with maximum draft at its outlet to be $h \approx 35\,m$*, so that the S-pipe will be subjected to the impulses* $F_L = F_R \approx 5384$ *tons at its inlet and outlet, as well as the resultant centrifugal forces* $\tilde{F}_{c1} = \tilde{F}_{c2} \approx 3760$ *tons at its two curved parts. Because of being non-collinear, each pair of impulses or centrifugal forces will induce an unbalanced "couple" with total magnitude* $C_{total} \approx 216727$ *m-ton, furthermore, its vibration due to pulsating fluid flow may lead to the liquefaction of soil contacting with it. Since the above-mentioned problems are neglected in the reviewed report, the first objective of this paper is to use the finite element method (FEM) for studying the quasi-static deflections of some points on the S-pipe due to actions of the "constant" impulses at its inlet and outlet as well as the centrifugal forces at the two curved parts when the flowing velocity becomes a "constant" (e.g.,* $V \approx 24.25$ *m/s) from the initial static condition (with* $V = 0$*). The next objective is to study the dynamic responses of the S-pipe due to "pulsating" flow with velocity* $V(t) = V_0(1 + ¢ \cos \mu_e t)$*, where* V_0 *is average velocity, t is time,* $¢$ *is pulsating parameter and* μ_e *is pulsating frequency. Numerical results reveal that the S-pipe will be safe if it is subjected to the "constant" impulses and centrifugal forces, however, its safety may be questionable if it is subjected to "pulsating" flow. It is believed that the original conception shown in the Appendix of this paper should be a better choice.*

KEYWORDS: *Centrifugal Force, Forced Vibration, Free Vibration, Impulse, Pulsating Flow, Soil Liquefaction*

Article History

Received: *16 Dec 2017* | ***Revised:*** *20 Dec 2017* | ***Accepted:*** *19 Jan 2018*

INTRODUTION

The studies on the dynamic problem of fluid-conveying pipes are more than 50 years (Ashley and Haviland, 1950; Housner, 1952; Long, 1955; Hsu, 1963), thus, the literature concerned is plenty. Since Ibrahim (2010, 2011) has reviewed several hundred references regarding pipes conveying fluids, only some pertinent articles are mentioned in this paper. For the bending vibrations of a fluid-conveying uniform *pipe* and that of a uniform *beam*, one of the main differences is that the former has the Coriolis force and the latter does not have. For this reason, even if the inner and outer dampings are equal to zero, the *r*th eigenvalue of a fluid-conveying *pipe* takes the form of complex number $\alpha_r = \alpha_{r,R} + j\alpha_{r,I}$, where $\alpha_{r,R}$ and $\alpha_{r,I}$ denote the real part and imaginary part of α_r, respectively, and $j = \sqrt{-1}$. Through theoretical analysis and model tests, Benjamin (1961a, 1961b) proved that the articulated fluid-conveying pipe has two types of instabilities, buckling and fluttering. The *buckling* instability appears when $\alpha_{r,R} > 0$ and $\alpha_{r,I} = 0$, while the *fluttering* instability occurs if $\alpha_{r,R} > 0$ and $\alpha_{r,I} \neq 0$. The last conclusion is the basis for the instability problem of fluid-conveying pipes. After Benjamin (1961a, 1961b), Gregory and Paidoussis (1966a, 1966b) studied the free vibration characteristics of a cantilevered fluid-conveying pipe and presented a "universal" stability curve. Since, for each curve, the "abscissa" is the dimensionless mass ratio $m_f^* = m_f/(m_f + m_p)$ and the "ordinate" is the dimensionless critical velocity $V_{cr}^* = V_{cr} L\sqrt{m_f/(EI)}$, the above-mentioned "universal" stability curve is available for the uniform fluid-conveying pipes with various pipe dimensions and material constants. However, the last statement is correct only for the Euler-Bernoulli pipe with the effects of shear deformation and rotary inertia neglected, and incorrect for the Timoshenko pipes that are dependent on the slenderness ratios. For a fluid-conveying pipe with the pulsating flow velocity $V(t) = V_0(1 + \gamma \cos \mu_e t)$ with V_0 denoting the average velocity, Chen (1971) used the Hsu's (1963) method to study the influence of pulsating parameter γ and pulsating frequency μ_e on the area of the instability region. Later, Paidoussis and Issid (1974) plotted the Argand diagrams to determine the critical flow velocity V_{cr} of the fluid-conveying pipe. From the existing literature (Paidoussis and Sundararajan, 1975; Paidoussis and Issid, 1976; Paidoussisand Laithier, 1976; Noah and Hopkins, 1980; Chen and Fan, 1987; Aldraihem, 2007; Yu et al., 2014; Wu et al., 2015), one sees that the problems studied in most existing works have something to do with the stability curves, Argand diagrams or area of instability region of the fluid-conveying pipes. It is also seen that most of the fluid-conveying pipes are single-span, and only a few of them are multi-span (Wu and Shih, 2001; Wu et al., 2015). Furthermore, most of the problems are solved with the classical analytical methods, and only a few of them are solved with the finite element method (FEM) (Kohli and Nakra, 1984; To and Healy, 1986; Chen and Fan, 1987; Sreejith et al., 2004; Aldraihem, 2007; Wu et al., 2015; Arguelles and Casanova, 2015).

It is similar to the railways (Wu and Shih, 2000a, 2000b) or ocean structures (Wu and Chang, 1988; Wu and Chen, 2010) that, for a fluid-conveying pipe imbedded in the soil, the interaction between pipe and soil may be modeled by the uniformly distributed springs with stiffness k_f (Lottati and Kornecki, 1986; Djondjorov et al., 2001; Ryu et al., 2004). Since the value of k_f is dependent on the property of soil (Richart et al., 1970) and must be determined by experiments, in this paper, it is provided by the company building the S-pipe. The last pipe is composed of five segments, including two curved (or arc) pipe segments and three straight ones, use of pure curved *pipe* theory (Chen, 1972, 1973) or pure curved *beam* theory (Wu and Chiang, 2003, 2004) for solving the dynamic problem of this S-pipe is very difficulty, thus, it is

solved with the conventional FEM (Kohli and Nakra, 1984; Przemieniecki, 1985; To and Healy, 1986; Chen and Fan, 1987; Sreejith et al., 2004; Aldraihem, 2007; Wu et al., 2015; Arguelles and Casanova, 2015) in this paper. Two types of flow velocity are studied: *constant* velocity V_0 and *pulsating* velocity $V(t) = V_0(1+¢\cos\mu_e t)$. For *constant* velocity V_0, the purpose is to study the "quasi-static" deflections of some points on the S-pipe due to actions of the *constant* impulses at the inlet and outlet as well as the *constant* centrifugal forces at the two curved parts. For *pulsating* velocity, the purpose is to study the dynamic responses of the above-mentioned points on the pipe. Numerical results reveal that the safety of the S-pipe may be questionable if it is subjected to *pulsating* flow and the original conception (with the S-pipe replaced by the siphon) should be safer, more efficient and more practical.

SKETCH OF THE S-PIPE

A sketch of the S-pipe is shown in Figure 1. It is a double-shell pipe with an inner diameter (of the inner shell) $d_i = 10$ m and outer diameter (of the outer shell) $d_o = 11.66$ m. The thickness of the inner shell is $t_{in} = 0.035$ m and that of the outer shell is $t_{out} = 0.032$ m. The entire pipe is composed of three straight pipe segments and two curved ones. For the last two curved (arc) segments, the radii of curvatures are $R_1 = 20$ m and $R_2 = 30$ m with subtended angles $\bar{}_1 = 40^o$ and $\bar{}_2 = 40^o$, respectively. In Figure 1, along the center line of the pipe, the arc denoted by $\overline{BCD}$ is the 1st curved pipe segment with *B* and *D* denoting its left and right ends, respectively, and *C* denoting its middle; similarly, the arc denoted by $\overline{EFG}$ is the 2nd curved pipe segment with *E* and *G* denoting its left and right ends, respectively, and *F* denoting its middle. Among the three straight pipe segments, two of them are at the left inlet denoted by $\overline{AB}$ and right outlet denoted by $\overline{GH}$, respectively, the third one is $\overline{DE}$ with its left end *D* connecting with the 1st curved pipe segment and its right end *E* is connecting with the 2nd curved pipe segment. It is noted that the straight pipe segment $\overline{DE}$ is tangent to the two curved pipe segments at *D* and *E*, respectively. Furthermore, the horizontal distance between left inlet and right outlet is about $L_x = 56.11$ m and the vertical one is about $L_y = 20$ m, and the corresponding elevations are: EL175m at the inlet and EL195m at the outlet. Since the maximum elevation of the free water surface of Tsen-Weng reservoir is EL230m, the maximum elevation head for the flowing water at the outlet of S-pipe is $h_{max} = 230 - 195 = 35$ m. Therefore, the variation of average flow velocity *V* for the S-pipe is shown in Table 1, where $g = 9.8$ m/s is the gravity acceleration and *h* is the water depth (draft) at the center of the pipe outlet.

Table 1: Influence of Draft *h* at Pipe Outlet on the Average Flowing Velocity *V* in the S-Pipe

Draft at Pipe Outlet, *h* (m)		**4**	**5**	**9**	**10**	**16**	**20**	**25**	**30**	**35**
$V = \sqrt{2gh}$	m/s	8.85	9.90	13.28	14.00	17.71	19.80	22.14	24.25	26.19
	km/h	31.87	35.64	47.81	50.40	63.75	71.27	79.68	87.29	94.28

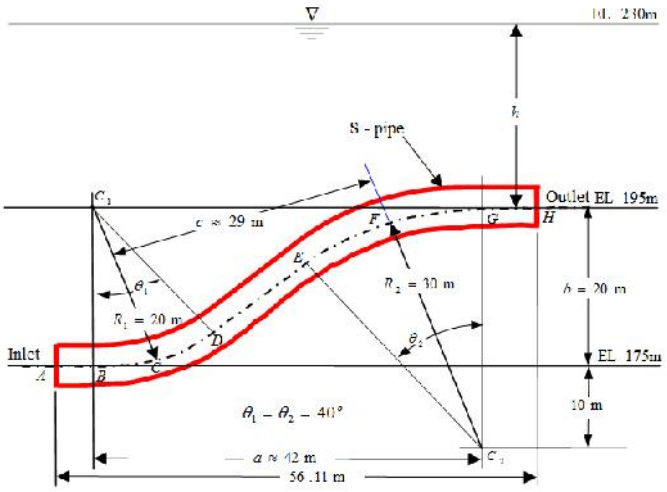

Figure 1: The Double-Shell S-Pipe with Inner Diameter (of the Inner Shell) $d_i = 10$ m and Outer Diameter (of the Outer Shell) $d_o = 11.66$ m, and Thickness of the Inner Shell $t_{in} = 0.035$ m and that of the Outer Shell $t_{out} = 0.032$ m. It is Composed of three *Straight* Pipe Segments and Two *Curved* Ones. The Outlet of the Pipe is Connected with an 1.2 km Tunnel Passing through a Mountain

FREE VIBRATION ANALYSIS BY FINITE ELEMENT METHOD (FEM)

In this paper, the vibration analysis of the S-pipe is conducted by using the finite element method (FEM). Some key points concerned are introduced as follows.

MATHEMATICAL MODEL

The mathematical model of the S-pipe studied in this paper is shown in Figure 2, in which, the entire pipe is considered as a free-clamped (F-C) curved beam rested on the elastic foundation with k_f denoting the "uniform-distributed" stiffness between the pipe and the soil.

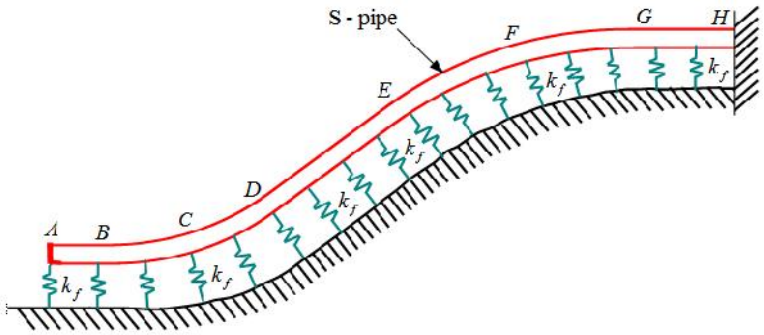

Figure 2: The S-Pipe is Modeled by a Free-Clamped (F-C) Curved Beam Rested on the Elastic Foundation with k_f Denoting the "Uniform-Distributed" Stiffness between the Pipe and the Soil

FINITE ELEMENT MODEL

According to the sketch of the S-pipe shown in Figure 1 and the mathematical model shown in Figure 2, a finite element model composed of 66 two-node pipe elements and 67 nodes is established as shown in Figure 3. From last figure one sees that the entire pipe is divided into 5 *segments*, among which, the 1st segment ($\overline{AB}$), 3rd segment ($\overline{DE}$) and 5th

segment ($\overline{GH}$) are the straight pipes to be subdivided into 5, 16 and 9 pipe *elements* (i.e., $n_{e,1}=5$, $n_{e,3}=16$ and $n_{e,5}=9$), respectively; while the 2nd segment ($\overline{BCD}$) and 4th segment ($\overline{EFG}$) are the curved pipes with subtended angles $\theta_1=\theta_2=40^o$ to be subdivided into 16 and 20 pipe elements (i.e., $n_{e,2}=16$ and $n_{e,4}=20$), respectively. For convenience, the last two curved pipes are called the 1st and 2nd curved pipe segments in this paper and their radii of curvatures are denoted by $R_1=20$ m and $R_2=30$ m, respectively. It is noted that, in Figure 3, the unit of lengths is meter (m).

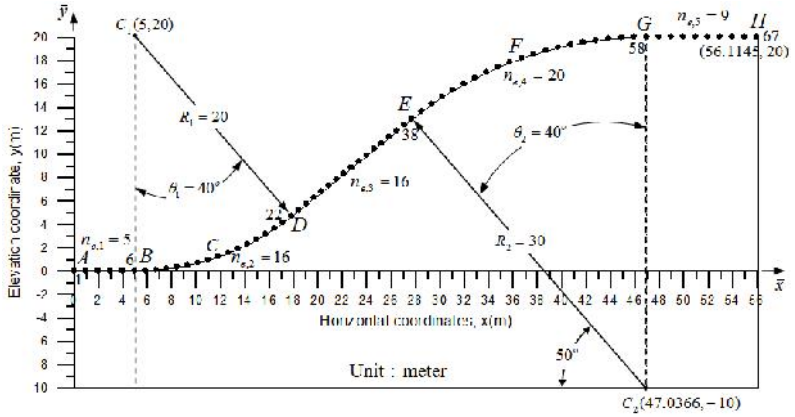

Figure 3: The Finite Elements along the Center Line of the S-Pipe: the Entire Pipe is Composed of Five Pipe *Segments* Including three Straight Ones ($\overline{AB}$, $\overline{DE}$ and $\overline{GH}$) and Two Curved Ones ($\overline{BCD}$ and $\overline{EFG}$), and the Total Numbers of Pipe *Elements* are $n_{e,i}=5$, 16, 16, 20 and 9, Respectively

ELEMENTAL PROPERTY MATRICES

Each pipe element composed of the entire S-pipe shown in Figure 3 is to take the form shown in Figure 4. It is a two-node clamped-clamped (C-C) beam element with each node having three displacements, u_1-u_3 and u_4-u_6. Among which, u_1 and u_4 are the longitudinal (or axial) displacements in the *x*-direction, u_2 and u_5 are the transverse (lateral) displacements in the *y*-direction, and u_3 and u_6 are the angular displacements (or rotational angles) about the *z*-axis, respectively. The mass matrix $[m]_e$, damping matrix $[c]_e$ and stiffness matrix $[k]_e$ of such a *pipe element* are given by (Kohli and Nakra, 1984; Przemieniecki, 1985; To and Healy, 1986; Wu et al., 2015)

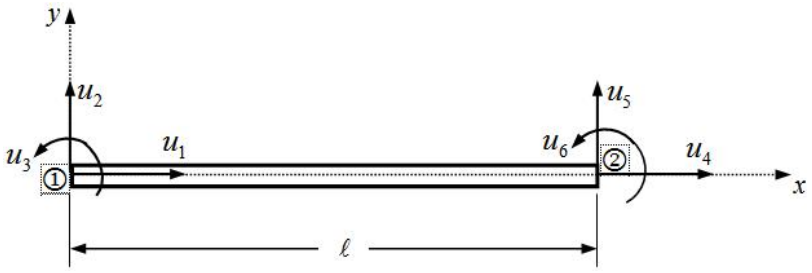

Figure 4: The Node Displacements of a Two-Node C-C Pipe Element with Six DOFs

$$[m]_e=\frac{(m_p+m_f+m_{add})\ell}{420}\begin{bmatrix}140 & & & & & \\ 0 & 156 & & & \text{Sym} & \\ 0 & 22\ell & 4\ell^2 & & & \\ 70 & 0 & 0 & 140 & & \\ 0 & 54 & 13\ell & 0 & 156 & \\ 0 & -13\ell & -3\ell^2 & 0 & -22\ell & 4\ell^2\end{bmatrix} \quad \textbf{(1)}$$

$$[c]_e = \frac{m_f V}{30}\begin{bmatrix} 0 & 0 & 0 & 0 & 0 & 0 \\ 0 & 0 & 6\ell & 0 & 30 & -6\ell \\ 0 & -6\ell & 0 & 0 & 6\ell & -\ell^2 \\ 0 & 0 & 0 & 0 & 0 & 0 \\ 0 & -30 & -6\ell & 0 & 0 & 6\ell \\ 0 & 6\ell & \ell^2 & 0 & -6\ell & 0 \end{bmatrix} \quad \textbf{(2)}$$

$$[k]_e = [k_B]_e + [k_F]_e + [k_G]_e \quad \textbf{(3)}$$

In Equation (3), the symbols $[k_B]_e$, $[k_F]_e$ and $[k_G]_e$ are the bending, elastic-foundation and geometric element stiffness matrices given by

$$[k_B]_e = \begin{bmatrix} EA/\ell & & & & & \\ 0 & 12EI/\ell^3 & & & \text{Sym} & \\ 0 & 6EI/\ell^2 & 4EI/\ell & & & \\ -EA/\ell & 0 & 0 & EA/\ell & & \\ 0 & -12EI/\ell^3 & -6EI/\ell^2 & 0 & 12EI/\ell^3 & \\ 0 & 6EI/\ell^2 & 2EI/\ell & 0 & -6EI/\ell^2 & 4EI/\ell \end{bmatrix} \quad \textbf{(4)}$$

$$[k_F]_e = \frac{k_f \ell}{420}\cdot\begin{bmatrix} 0 & & & & & \\ 0 & 156 & & & \text{Sym} & \\ 0 & 22\ell & 4\ell^2 & & & \\ 0 & 0 & 0 & 0 & & \\ 0 & 54 & 13\ell & 0 & 156 & \\ 0 & -13\ell & -3\ell^2 & 0 & -22\ell & 4\ell^2 \end{bmatrix} \quad \textbf{(5)}$$

$$[k_G]_e = \left(\frac{P}{30\ell}\right)\cdot\begin{bmatrix} 30 & & & & & \\ 0 & 36 & & & \text{Sym} & \\ 0 & 3\ell & 4\ell^2 & & & \\ -30 & 0 & 0 & 30 & & \\ 0 & -36 & -3\ell & 0 & 36 & \\ 0 & 3\ell & -\ell^2 & 0 & -3\ell & 4\ell^2 \end{bmatrix} \quad \textbf{(6)}$$

where

$$P = P_p + p_f A_f + m_f V^2 \quad \textbf{(7)}$$

In the right side of Equation (7), P_p is the axial load applied on the pipe wall, $p_f A_f$ is the fluid pressure on the pipe section and $m_f V^2$ is the centrifugal force on the pipe section due to structure vibrations. Where the compressions are positive (+) and tensions are negative (-). Furthermore, the centrifugal forces induced by the 1st and 2nd *curved* pipe segments ($\overline{BCD}$ and $\overline{EFG}$) are considered as the external loads on the entire S-pipe and are not included in Equation (7), because each pipe element shown in Figure 3 is replaced by the *straight* one. The definitions for the other symbols appearing in Eqs. (1)-(7) are as follows: m_p = pipe mass per unit length (including pipe material and cement in the ballast tanks), m_f = fluid mass per unit pipe length in the pipe, m_{add} = added mass (of water) per unit length surrounding the

pipe, $V = V_0$ = average flowing velocity of fluid, ℓ = length of each pipe element, E = Young modulus of pipe material, A = cross-sectional area of pipe *wall*, A_f = cross-sectional area of fluid column in the pipe, I = moment of inertia of cross-sectional area A, k_f = stiffness of soil for per unit pipe length, and P_p = axial pressure on the pipe *wall*.

TRANSFORMATION MATRIX

From the finite element model shown in Figure 3 one sees that, besides the first five pipe elements ($n_{e,1} = 5$) near the inlet and the final 9 ones ($n_{e,5} = 9$) near the outlet, the local coordinate systems oxy for all the other pipe elements are not parallel to the global coordinate system $\overline{oxy}$ for the entire pipe such as shown in Figure 5. Thus, the property matrices of most pipe elements must be transformed into the corresponding ones in terms of the global coordinate system before they are assembled to give the overall ones. For this reason, the transformation matrix $[^a]$ is introduced as follows (Wu, 2013)

$$[^a] = \left[\begin{array}{ccc:ccc} \cos\sim & \sin\sim & 0 & 0 & 0 & 0 \\ -\sin\sim & \cos\sim & 0 & 0 & 0 & 0 \\ 0 & 0 & 1 & 0 & 0 & 0 \\ \hdashline 0 & 0 & 0 & \cos\sim & \sin\sim & 0 \\ 0 & 0 & 0 & -\sin\sim & \cos\sim & 0 \\ 0 & 0 & 0 & 0 & 0 & 1 \end{array}\right] \tag{8}$$

where

$$\cos\sim = \Delta x/\ell\,,\ \sin\sim = \Delta y/\ell \tag{9a,b}$$

$$\Delta x = \bar{x}_2 - \bar{x}_1\,,\ \Delta y = \bar{y}_2 - \bar{y}_1\,,\ \ell = \sqrt{(\Delta x)^2 + (\Delta y)^2} \tag{10a,b,c}$$

In the above equations, $\sim$ is the angle between the positive local x-axis and the positive global $\bar{x}$-axis, while $(\bar{x}_1, \bar{y}_1)$ and $(\bar{x}_2, \bar{y}_2)$ are the global coordinates of the 1st node ① and 2nd node ② of the pipe element, respectively. It is evident that the symbol ℓ given by Equation (10c) denotes the length of the pipe element.

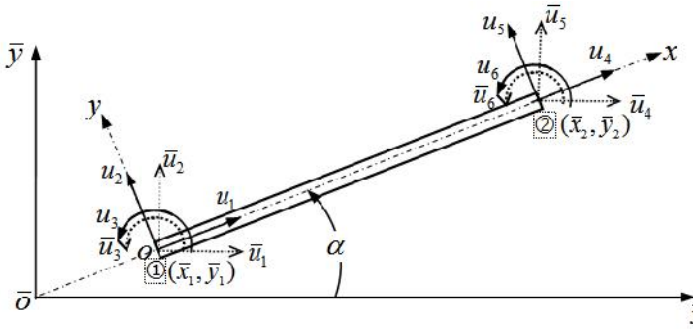

Figure 5: The Node Displacements of a C-C Pipe Element with Respect to the Local *Oxy* Coordinate System, u_i ($i = 1-6$), and the Corresponding Ones with Respect to the Global $\overline{oxy}$ Coordinate System, $\bar{u}_i$ ($i = 1-6$)

Now, the element property matrices $[a]_e$ with respect to the local *oxy* coordinate system given by Eqs. (1)-(6) can be transformed into the corresponding ones $[\bar{a}]_e$ respect to the global $\overline{oxy}$ coordinate system by using

$$[\bar{a}]_e = [\mathtt{a}]^T [a]_e [\mathtt{a}] \tag{11}$$

where $[a]_e = [m]_e, [c]_e, [k_B]_e, [k_F]_e$ or $[k_G]_e$, while $[\bar{a}]_e = [\bar{m}]_e, [\bar{c}]_e, [\bar{k}_B]_e, [\bar{k}_F]_e$ or $[\bar{k}_G]_e$.

DETERMINATION OF UN-DAMPED NATURAL FREQUENCIES AND MODE SHAPES

The equations of motion for the *entire* S-pipe take the form

$$[\bar{m}]\{\ddot{\bar{u}}\} + [\bar{c}]\{\dot{\bar{u}}\} + [\bar{k}]\{\bar{u}\} = \{\bar{F}\} \tag{12a}$$

where $[\bar{m}]$, $[\bar{c}]$ and $[\bar{k}]$ are the overall mass, damping and stiffness matrices of the entire pipe system and $\{\bar{F}\}$ is the overall external loading vector. For free vibrations, one has $\{\bar{F}\} = 0$, thus, Equation (12a) becomes

$$[\bar{m}]\{\ddot{\bar{u}}\} + [\bar{c}]\{\dot{\bar{u}}\} + [\bar{k}]\{\bar{u}\} = 0 \tag{12b}$$

If the damping effect is neglected, then $[\bar{c}] = 0$, and Equation (12b) reduces to

$$[\bar{m}]\{\ddot{\bar{u}}\} + [\bar{k}]\{\bar{u}\} = 0 \tag{12c}$$

Which is the standard equation of motion for an *un-damped* free vibration system and can be solved for the natural frequencies and mode shapes using the generalized Jacobi method (Bathe, 1982; Wu, 2013).

DETERMINATION OF DAMPED NATURAL FREQUENCIES AND MODE SHAPES

Equation (12b) is the equation of motion for a *damped* free-vibration system. Due to the existence of damping term, application of the existing computer codes (Garbow, 1977) requires that Equation (12b) must be transformed into the form below (Meirovitch, 1967; Wu et al., 2015)

$$[\bar{M}]\{\dot{\bar{U}}\} + [\bar{K}]\{\bar{U}\} = 0 \tag{13}$$

where

$$[\bar{M}] = \begin{bmatrix} [0] & [\bar{m}] \\ [\bar{m}] & [\bar{c}] \end{bmatrix},\ [\bar{K}] = \begin{bmatrix} -[\bar{m}] & [0] \\ [0] & [\bar{k}] \end{bmatrix},\ \{\bar{U}\} = \begin{Bmatrix} \{\dot{\bar{u}}\} \\ \{\bar{u}\} \end{Bmatrix},\ \{\dot{\bar{U}}\} = \begin{Bmatrix} \{\ddot{\bar{u}}\} \\ \{\dot{\bar{u}}\} \end{Bmatrix} \tag{14a-d}$$

With each specified flowing velocity V, the rth eigenvalues μ_r and the associated rth eigenvectors $[\phi_r]$ of Equation (13) take the pairs of conjugate complex forms

$$\mu_r = \mu_{r,R} \pm j\mu_{r,I},\ \{\phi_r\} = \begin{Bmatrix} \mu_{r,R}\phi_{r,R} \\ \phi_{r,R} \end{Bmatrix} \pm j \begin{Bmatrix} \mu_{r,I}\phi_{r,I} \\ \phi_{r,I} \end{Bmatrix} \tag{15a,b}$$

In the above equations, the subscripts, *R* and *I*, refer to "real" and "imaginary" parts of the complex numbers, respectively, and $j = \sqrt{-1}$. Furthermore, the "imaginary" part of μ_r, $\mu_{r,I}$, denotes the rth natural frequency and the corresponding "real" part of $\{\phi_r\}$, $\{\phi_{r,R}\}$, denotes the rth mode shape. Numerical results reveal that $\{\phi_{r,R}\} \neq \{\phi_{r,I}\}$, this may be due to $\mu_{r,R} \neq \mu_{r,I}$.

It is similar to the C-F pipe with free end at *downstream* (Chen and Fan, 1987; Aldraihem, 2007; Wu et al., 2015) that, for the F-C pipe studied in this paper, the following momentum transport at the *upstream* free end must be considered: $-m_f V^2 \bar{u}_y' - m_f V \dot{\bar{u}}_y \,|_{\bar{x}=0}$.

FORCED VIBRATION ANALYSIS BY FINITE ELEMENT METHOD

In this section, the forced dynamic responses of the free-clamped (F-C) S-pipe subjected to the flow-induced impulsive forces at inlet and outlet and the centrifugal forces (CFs) at the 1st and 2nd curved pipe segments are studied. The centrifugal force per unit pipe length induced by the water flowing through the curved pipe segments is given by

$$F_c' = \rho_w A_w V^2 / R \tag{16}$$

where $\rho_w = \rho_f$ is the mass density of water, $A_w = A_f$ is the cross-section area of water column inside the pipe, V is average flow velocity and R is the radius of curvature of the curved pipe segment.

If the symbols n_{c1} and n_{c2} denote the total numbers of arc elements composing of the 1st and 2nd curved pipe segments, respectively, while $\bar{\Delta}_1$ and $\bar{\Delta}_2$ denote the subtended angles for each of the arc elements, then

$$\bar{\Delta}_1 = \bar{\theta}_1 / n_{c1} = 40^o / 16 = 2.5^o \,,\ \bar{\Delta}_2 = \bar{\theta}_2 / n_{c2} = 40^o / 20 = 2^o \tag{17a,b}$$

Where $\bar{\theta}_1 = 40^o$ and $\bar{\theta}_2 = 40^o$ are the subtended angles for the first and second curved pipe segments, respectively, while $n_{c1} = n_{e,2} = 16$ and $n_{c2} = n_{e,4} = 20$ as one may see from Figure 3.

If the node numbering for the 1st node in the 1st curved pipe segment is denoted by $n_{c1,L}$, then the angle $\bar{\theta}_{1,i}$ between the centrifugal force F_{c1i} and the negative $\bar{y}$-axis is determined by (cf. Figure 6)

$$\bar{\theta}_{1,i} = (n_i - n_{c1,L}) \cdot \bar{\Delta}_1 \tag{18}$$

In Figure 6, $\bar{o}\bar{x}\bar{y}$ is the global coordinate system with origin $\bar{o}$ at the inlet of the S-pipe.

Similarly to Equation (18), if the node numbering for the 1st node in the 2nd curved pipe segment is denoted by $n_{c2,L}$, then the angle $\bar{\theta}_{2,i}$ between the centrifugal force F_{c2i} and the positive $\bar{y}$-axis is determined by

$$\bar{\theta}_{2,i} = \bar{\theta}_2 - [(n_i - n_{c2,L}) \cdot \bar{\Delta}_2] = 40^o - [(n_i - n_{c2,L}) \cdot \bar{\Delta}_2] \tag{19}$$

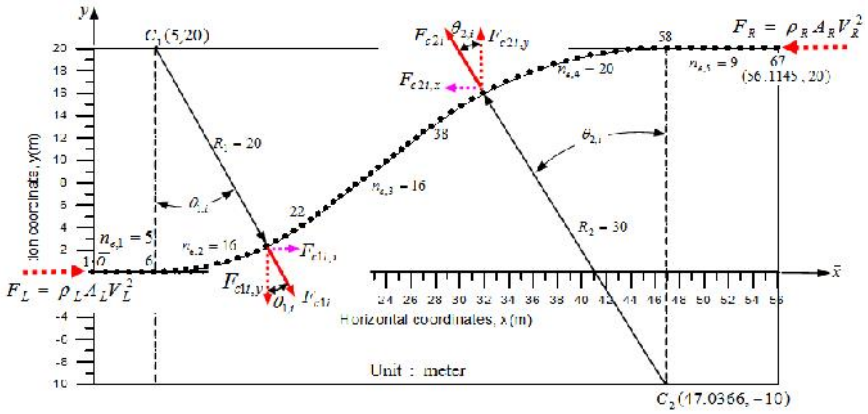

Figure 6: The Centrifugal Force F_{c1i} at *i*th Node in the 1st Curved Pipe Segment with Angle $\bar{}_{1,i}$ with the $-\bar{y}$ Axis and its Components, $F_{c1i,x}$ and $F_{c1i,y}$, in $\bar{x}$ and $\bar{y}$ Directions, Respectively, and the Corresponding Ones at *i*th Node in the 2nd Curved Pipe Segment with Angle $\bar{}_{2,i}$ with the $+\bar{y}$ Axis, F_{c2i}, $F_{c2i,x}$ and $F_{c2i,y}$. In Addition, $F_L = \rho_L A_L V_L^2$ and $F_R = \rho_R A_R V_R^2$ are the Impulsive Forces of the Flowing Fluid on the *Left* Inlet and *Right* Outlet of the Pipe, Respectively

Based on the angle $\bar{}_{1,i}$ between each centrifugal force F_{c1i} and negative $\bar{y}$-axis given by Equation (18) for the 1st curved pipe segment and the corresponding one $\bar{}_{2,i}$ for the 2nd curved pipe segment, one may obtain the following centrifugal force components in $\bar{x}$-direction and those in $\bar{y}$-direction (cf. Figure 6)

$$F_{c1i,x} = +F_{c1i}\sin\bar{}_{1,i},\ F_{c1i,y} = -F_{c1i}\cos\bar{}_{1,i}\ (\text{for } i = n_{c1,L} \text{ to } (n_{c1,L}+n_{c1})) \tag{20a,b}$$

$$F_{c2i,x} = -F_{c2i}\sin\bar{}_{2,i},\ F_{c2i,y} = +F_{c2i}\cos\bar{}_{2,i}\ (\text{for } i = n_{c2,L} \text{ to } (n_{c2,L}+n_{c2})) \tag{21a,b}$$

Since the centrifugal force per unit length, F_c', is given by Equation (16), the distributed centrifugal node forces appearing in Eqs. (20a,b) and (21a,b) are determined by

$$F_{c1i} = F_c' \cdot R_1 \Delta\bar{}_1 = \rho_w A_w V^2 \cdot \Delta\bar{}_1\ (\text{for } i = (n_{c1,L}+1) \text{ to } (n_{c1,L}+n_{c1}-1)) \tag{22a}$$

$$F_{c2i} = F_c' \cdot R_2 \Delta\bar{}_2 = \rho_w A_w V^2 \cdot \Delta\bar{}_2\ (\text{for } i = (n_{c2,L}+1) \text{ to } (n_{c2,L}+n_{c2}-1)) \tag{23a}$$

Eqs. (22a) and (23a) give the intermediate-node forces, and those at the two ends of the 1st and 2nd curved pipe segments are given by

$$F_{c1i} = \tfrac{1}{2}\rho_w A_w V^2 \cdot \Delta\bar{}_1\ (\text{for } i = n_{c1,L} \text{ or } n_{c1,L}+n_{c1}) \tag{22b}$$

$$F_{c2i} = \tfrac{1}{2}\rho_w A_w V^2 \cdot \Delta\bar{}_2\ (\text{for } i = n_{c2,L} \text{ or } n_{c2,L}+n_{c2}) \tag{23b}$$

It is noted that, in Eqs. (22a,b) and (23a,b), the units of $\Delta\bar{}_1$ and $\Delta\bar{}_2$ are "radian".

RAYLEIGH DAMPING MATRIX

Since the damping matrix $[\bar{c}]$ appearing in Equation (12a) contains the effect of Coriolis force only, a Rayleigh damping matrix to include the overall damping effect of the entire S-pipe is introduced here, which is to take the form (Bathe, 1982; Wu, 2013)

$$[\hat{c}] = a[\overline{m}] + b[\overline{k}] \tag{24a}$$

where $[\overline{m}]$ and $[\overline{k}]$ are the overall mass matrix and stiffness matrix, respectively, while a and b are constants determined by

$$a = \frac{2\mu_i\mu_j(\P_i\mu_j - \P_j\mu_i)}{\mu_j^2 - \mu_i^2}, \quad b = \frac{2(\P_j\mu_j - \P_i\mu_i)}{\mu_j^2 - \mu_i^2} \tag{24b,c}$$

In the above two expressions, $\P_i$ and $\P_j$ are the damping ratios corresponding to the two natural frequencies μ_i and μ_j, respectively, for $\mu_i < \mu_j$. In such a case, Equation (12a) becomes

$$[\overline{m}]\{\ddot{\overline{u}}\} + ([\overline{c}] + [\hat{c}])\{\dot{\overline{u}}\} + [\overline{k}]\{\overline{u}\} = \{\overline{F}\} \tag{25}$$

Even if the effect of $[\overline{c}]$ due to Coriolis force is considered, from the subsequent studies, one may find that the forced vibration responses will become very large if one sets $[\hat{c}] = 0$, because of neglecting the structural damping (i.e., $\P_i = \P_j = 0$).

NUMERICAL RESULTS AND DISCUSSIONS

In the finite element analysis, one of the tedious works is the preparation of input data. Thus, in this section, the determinations of global coordinates for the 67 nodes of the entire S-pipe and the other associated given data are introduced first. Next, the free and forced vibration-analysis results are followed.

As shown in Figure 3, the entire finite element model along the center line of the S-pipe is composed of five pipe *segments* including three straight ones ($\overline{AB}$, $\overline{DE}$ and $\overline{GH}$) and two curved ones ($\overline{BCD}$ and $\overline{EFG}$), and the total numbers of pipe *elements* are $n_{e,i} = 5$, 16, 16, 20 and 9, respectively. Where the lengths of elements in each pipe segment are equal to each other (but the length of each element in one pipe segment is different from that in the other pipe segment). Based on the above statements and the following information regarding the global coordinates of some key nodes, $A(0,0)$, $B(5,0)$, $D(17.856, 4.679)$, $E(27.716, 12.981)$, $G(47, 20)$ and $H(56, 20)$, one can obtain the global coordinates of all nodes by using computer.

The other associated given data are as follows: inner diameter of the double-shell pipe: $d_i = 10\,\text{m}$ (or radius $r_i = 5.0$ m); outer diameter of the double-shell pipe: $d_0 = 11.66\,\text{m}$ (or radius $r_o = 5.83$ m); thickness of inner shell: $t_{\text{in}} = 0.035\,\text{m}$; thickness of outer shell: $t_{\text{out}} = 0.032\,\text{m}$; Young's modulus: $E = 200\,\text{Gpa} = 2.0\times10^{11}\ \text{N/m}^2$; shear modulus: $G = 79.3\,\text{Gpa} = 0.793\times10^{11}\ \text{N/m}^2$; mass density of pipe shells: $\°_p = 7850\,\text{kg/m}^3$; mass density of water: $\°_w = 1000\ \text{kg/m}^3$; stiffness of soil: $k_f \approx 203.6\times10^6\ \text{N/m}^2$; total pipe length: $L = 61.795\,\text{m}$; total pipe mass: $m = 20.52289\times10^6$ kg (including mass of cement in ballast tanks); pipe mass per unit length: $m' = m/L = 0.3321125\times10^6$ kg/m (Theoretical value: $m' = \°_p A_{wall} = 17838.18\,\text{kg/m} = 0.1783818\times10^5\,\text{kg/m}$); pipe's added mass per unit length: $m'_a = \°_w A_o = \°_w(\®d_o^2/4) = 106779.273\,\text{kg/m}$. The polar moments of inertia for the cross-sectional area of the outer and inner shells are $I_{x,o} = I_{p,out} = \frac{\®}{32}[D_{o,2}^4 - D_{o,1}^4] = 39.51466\,\text{m}^4$ and

$I_{x,i} = I_{p,in} = \frac{\pi}{32}[(D_{i,2}^4 - D_{i,1}^4] = 27.77892\,\mathrm{m}^4$. Thus, the moment of inertia of the entire double-shell pipe about *y*- or *z*- axis is $I_y = I_z = \frac{1}{2}(I_{x,o} + I_{x,i}) = 33.64679\,\mathrm{m}^4$.

In the foregoing expressions, the values of soil stiffness k_f and total pipe mass *m* are obtained from measurements and provided by the company building the S-pipe.

FREE VIBRATION ANALYSIS

In this subsection, the influence of mass density $\rho_w = \rho_f$ and flowing velocity *V* of fluid on the natural frequencies and the associated mode shapes is studied.

Influence of Mass Density of Fluid on Free Vibration Characteristics

From Table 1 one sees that if the draft $h = 30$ m (at the outlet of the S-pipe) is selected to estimate the maximum flowing velocity of fluid in the pipe, then one has $V = 24.25$ m/s. In such condition, the lowest five natural frequencies μ_r (r/s) of the free-clamped (F-C) pipe are listed in Table 2 with the fluid mass densities ρ_w to be 1000 and 2000 $\mathrm{kg/m}^3$, respectively. For the case of damping effect due to Coriolis force to be considered, the eigenvalues of the S-pipe are the complex numbers of the form $\mu_r = \mu_{r,R} \pm j\mu_{r,I}$, thus, in addition to the imaginary parts $\mu_{r,I}$ corresponding to the conventional un-damped natural frequencies μ_r, the real parts $\mu_{r,R}$ are also listed in the parentheses of Table 2, because they influence the dynamic stability of a fluid-conveying pipe. From Table 2, one sees that:

- No matter the fluid mass density ρ_w = 1000 or 2000 $\mathrm{kg/m}^3$, the damped natural frequency $\mu_{r,I}$ is less than the corresponding un-damped one μ_r ($r = 1-5$), except the 2nd and 5th ones due to the *negative* damping effect of Coriolis force. However, the influence of Coriolis force is negligible. Since the real parts of all eigenvalues, $\mu_{r,R}$, listed in the parentheses of Table 2 are negative, the dynamic instability due to Coriolis force will not occur for the present S-pipe.
- With ρ_w = 1000 $\mathrm{kg/m}^3$, the corresponding lowest five mode shapes are shown in Figure 7(a) for the un-damped pipe and in Figure 7(b) for the damped pipe. Because the *un-damped* natural frequencies μ_r ($r = 1-5$) are very close to the corresponding *damped* ones $\mu_{r,I}$ as shown in Table 2, the un-damped mode shapes shown in Figure 7(a) are very close to the corresponding damped ones shown in Figure 7(b), except the 5th mode shapes.

Table 2: The Lowest Five *Un-Damped* Natural Frequencies μ_r and *Damped* Ones $\mu_{r,I}$ of the S-Pipe Conveying Fluid with Velocities $V = 24.25$ m/s

Conditions		Natural Frequencies, μ_r or $\mu_{r,I}$ (rad/s)				
Mass density of fluid (kg/m^3)	Damping effect (Coriolis force)	μ_1 or $\mu_{1,I}$ ($\mu_{1,R}$)	μ_2 or $\mu_{2,I}$ ($\mu_{2,R}$)	μ_3 or $\mu_{3,I}$ ($\mu_{3,R}$)	μ_4 or $\mu_{4,I}$ ($\mu_{4,R}$)	μ_5 or $\mu_{5,I}$ ($\mu_{5,R}$)
$\rho_w = 1000$	Neglected (un-damped)	18.7589	21.1909	31.3601	62.2232	71.9840
	Considered (damped)	18.7527 (-0.0891)	21.1931 (-0.0064)	31.3516 (-0.1447)	62.2177 (-0.1156)	71.9842 (-0.0006)
$\rho_w = 2000$	Neglected (un-damped)	16.0995	18.1799	26.9137	53.3912	61.7632
	Considered (damped)	16.0872 (-0.1311)	18.1850 (-0.0095)	26.8989 (-0.2131)	53.3815 (-0.1702)	61.7637 (-0.0009)

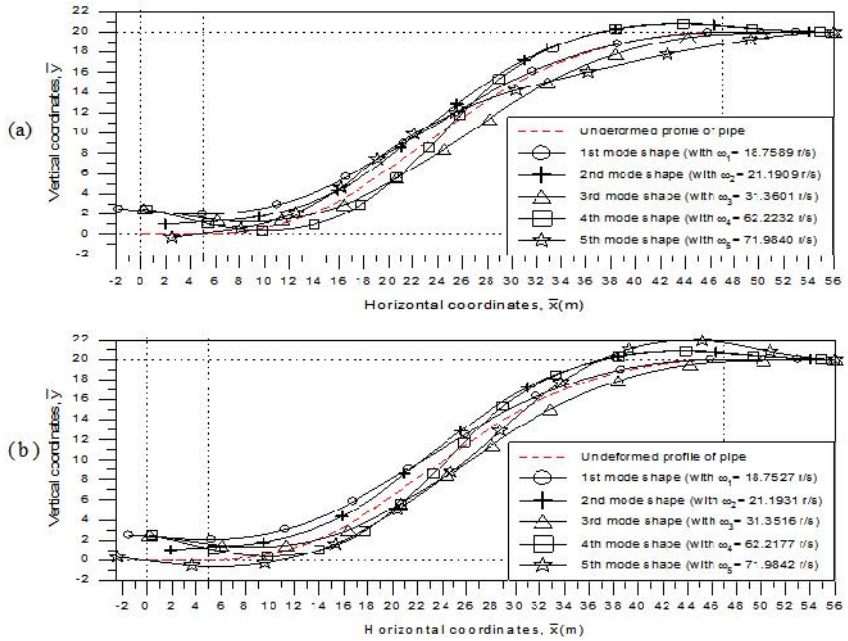

Figure 7: The Lowest Five Mode Shapes of the S-Pipe Conveying Fluid with Velocity $V = 24.25$ m/s and Mass Density $\rho_w = 1000$ kg/m^3 for the Cases of Coriolis -Force (Damping) effect: (a) Neglected and (b) Considered

Influence of Flowing Velocity on Free Vibration Characteristics

The influence of flowing velocity V of fluid on the property matrices of a pipe element is to appear in Equation (2) for the damping matrix due to Coriolis force and in Equation (7) for the centrifugal force associated with geometric stiffness matrix given by Equation (6). In Table 3, the 3rd row lists the lowest five natural frequencies of the pipe for the case of $V = 0$. From Table 3 one sees that, for the cases of $V = 10 - 30$ m/s, the influence of flowing velocity on the lowest five natural frequencies is small. For the "un-damped" natural frequencies μ_r of the pipe, the row before the final one of Table 3 indicates that μ_1 and μ_3 "increase" with the increase of flowing velocity V, and this trend is reverse for the μ_2, μ_4 and μ_5. Furthermore, all the "damped" natural frequencies $\mu_{r,I}$ "decrease" with increasing the flowing velocity as shown in the final row of Table 3. Since the real parts of all eigenvalues, $\mu_{r,R}$, listed in the parentheses of Table 3, are negative, the dynamic instability due to Coriolis force will not occur for the present S-pipe. This conclusion agrees with

that obtained from Table 2.

Table 3: The Lowest Five *Un-Damped* Natural Frequencies μ_r and *Damped* Ones $\mu_{r,I}$ of the S-Pipe Conveying Fluid with Mass Density $°_w = 1000$ kg/m^3 and Velocities $V = 0$, 10, 15, 20, 25 and 30 m/s, Respectively

Conditions		Natural Frequencies, μ_r or $\mu_{r,I}$ (rad/s)				
Flowing Velocity, V (m/s)	Damping effect (Coriolis force)	μ_1 or $\mu_{1,I}$ ($\mu_{1,R}$)	μ_2 or $\mu_{2,I}$ ($\mu_{2,R}$)	μ_3 or $\mu_{3,I}$ ($\mu_{3,R}$)	μ_4 or $\mu_{4,I}$ ($\mu_{4,R}$)	μ_5 or $\mu_{5,I}$ ($\mu_{5,R}$)
0	—	18.7554	21.1950	31.3551	62.2245	71.9893
10	Neglected (un-damped)	18.7560	21.1943	31.3560	62.2243	71.9884
	Considered (damped)	18.7550 (-0.0367)	21.1947 (-0.0026)	31.3545 (-0.0596)	62.2233 (-0.0476)	71.9885 (-0.0003)
15	Neglected (un-damped)	18.7568	21.1935	31.3570	62.2240	71.9873
	Considered (damped)	18.7544 (-0.0551)	21.1943 (-0.0039)	31.3538 (-0.0895)	62.2219 (-0.0715)	71.9874 (-0.0004)
20	Neglected (un-damped)	18.7578	21.1922	31.3585	62.2236	71.9857
	Considered (damped)	18.7536 (-0.0734)	21.1937 (-0.0053)	31.3527 (-0.1194)	62.2199 (-0.0953)	71.9858 (-0.0005)
25	Neglected (un-damped)	18.7591	21.1907	31.3604	62.2232	71.9837
	Considered (damped)	18.7525 (-0.0918)	21.1930 (-0.0066)	31.3514 (-0.1492)	62.2173 (-0.1191)	71.9838 (-0.0006)
30	Neglected (un-damped)	18.7607	21.1887	31.3628	62.2226	71.9812
	Considered (damped)	18.7513 (-0.1102)	21.1921 (-0.0080)	31.3498 (-0.1790)	62.2141 (-0.1430)	71.9814 (-0.0008)
Trend of frequencies	Un-damped	Increasing	Decreasing	Increasing	Decreasing	Decreasing
	Damped	Decreasing				

FORCED VIBRATION ANALYSIS

The objective of this section is to study the dynamic responses of the S-pipe due to actions of the *impulsive forces* and the *centrifugal forces* induced by the flowing fluid with velocity

$$V(t) = V_0(1 + ¢\cos \mu_e t) \tag{26}$$

For convenience, the following numerical values are used:

$$V_0 = 24.25 \text{ m/s (or } h = 30 \text{ m)},\ °_w = 1500 \text{ kg/m}^3,\ \mu_e = 1 - 36 \text{ rad/s},\ ¶_1 = ¶_2 = 0.05 \tag{27}$$

Time Histories of Displacements at Nodes 1 and 38

Based on the conditions given by Equation (27) with pulsating frequency $\mu_e = 10$ rad/s and pulsating parameter $¢ = 0$, the time histories for the displacements of nodes 1 and 38 in the horizontal ($\bar{x}$) direction, $u_1(t)$ and $u_{112}(t)$, are shown in Figure 8(a), and the corresponding ones in the vertical ($\bar{y}$) direction, $u_2(t)$ and $u_{113}(t)$, are shown in Figure 8(b). It is seen that all curves become the horizontal lines after time $t \geq 7$ seconds due to the effect of pipe's structural damping. Since the pulsating parameter is $¢ = 0$ for Figure 8, the ordinates corresponding to the last horizontal lines are,

respectively, called the "quasi-static deflections" (Δx or Δy) of the S-pipe at the specified nodes in the horizontal ($\bar{x}$) or vertical ($\bar{y}$) directions due to actions of the "constant" fluid *impulses* at the inlet and outlet as well as the *centrifugal forces* at the 1st and 2nd curved pipe segments. From Figure 8(a), one sees that $\Delta_{1x} \approx 0.021\,\text{m}$ and $\Delta_{38x} \approx 0.0049\,\text{m}$. Similarly, from Figure 8(b), one sees that $\Delta_{1y} \approx -0.021\,\text{m}$ and $\Delta_{38y} \approx 0.0035$ m. It is noted that all "quasi-static deflections" are positive (either rightward or upward) except Δ_{1y} (downward).

If all the foregoing conditions are kept unchanged except that the pulsating parameter of flowing velocity is replaced by $¢ = 0.2$ (instead of $¢ = 0$), then the time histories of displacements at nodes 1 and 38 are shown in Figure 9(a) for the horizontal ($\bar{x}$) displacements, $u_1(t)$ and $u_{112}(t)$, and in Figure 9(b) for the vertical ($\bar{y}$) displacements, $u_2(t)$ and $u_{113}(t)$. It is under our expectation that all curves become those of harmonic motions with respect to their "quasi-static" equilibrium positions (q-SEPs) after time $t \geq 7$ seconds, because the influences of all initial velocities have been damped out.

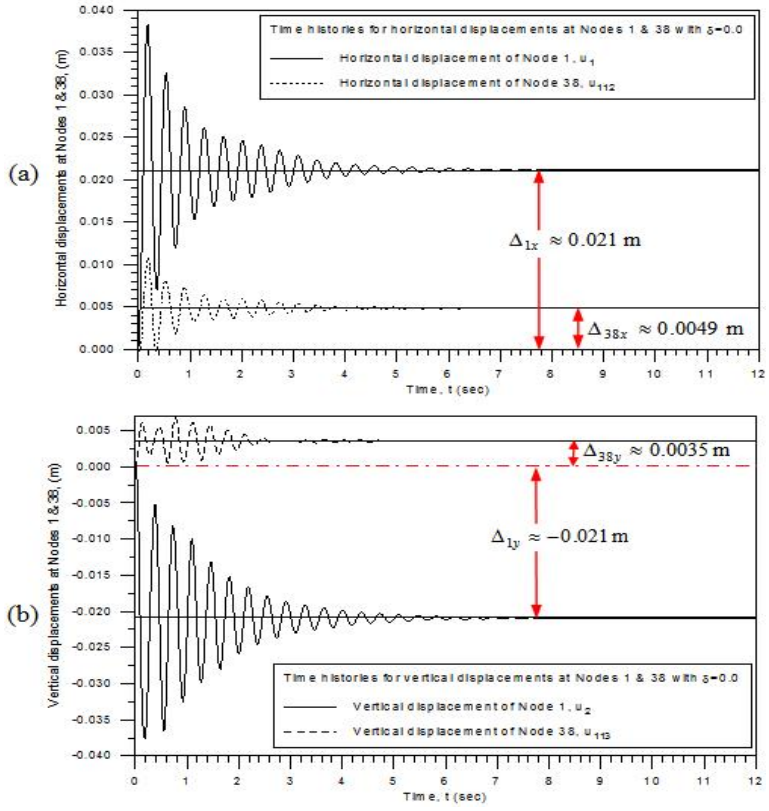

Figure 8: For the Case of $¢ = 0$, $\mu_e = 10$ Rad/s, $°_w = 1500\ \text{kg/m}^3$, $V_0 = 24.25$ m/s and $¶_1 = ¶_2 = 0.05$, the time Histories of Displacements at Nodes 1 and 38: (a) Horizontal ($\bar{x}$) Displacements, $u_1(t)$ and $u_{112}(t)$; (b) Vertical ($\bar{y}$) Displacements, $u_2(t)$ and $u_{113}(t)$

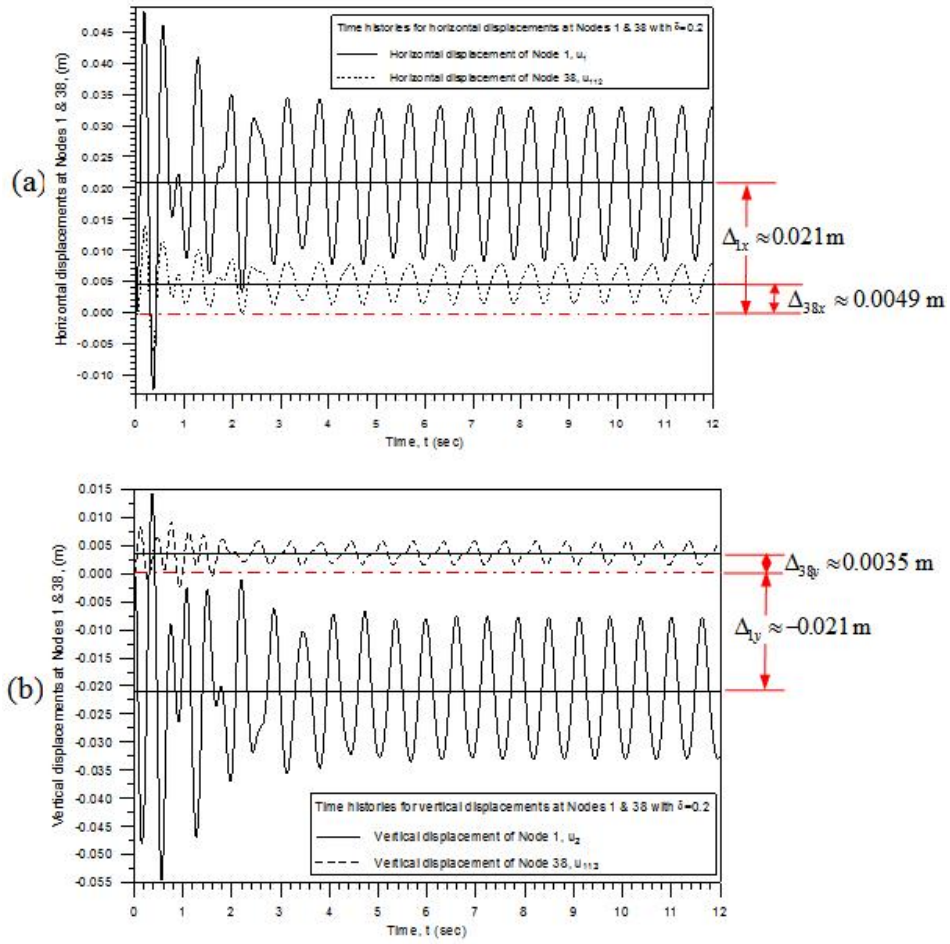

Figure 9 : All Legends are the Same as Figure 8 Except that $¢ = 0.2$ (Instead of $¢ = 0$)

Frequency-Response Amplitude Curves for Nodes 1 and 38

For the conditions given by Equation (27), the lowest five un-damped natural frequencies of the S-pipe are: 17.2773, 19.5136, 28.8829, 57.3030 and 66.2902 rad/s, respectively. Based on the *centrifugal* forces (CFs) on the 1st and 2nd curved pipe segments along with the *impulsive* forces on the inlet and outlet of the pipe shown in Figure 6, the frequency-response amplitude curves due to $¢ = 0.2$ and 0.4 are as follows:

For the case of $¢ = 0.2$, the frequency-response amplitude curves for nodes 1 and 38 are shown in Figure 10(a) for the horizontal ($\bar{x}$) displacement amplitudes, $|u_1(t)|_{\max}$ and $|u_{112}(t)|_{\max}$, and in Figure 10(b) for the vertical ($\bar{y}$) displacement amplitudes, $|-u_2(t)|_{\max}$ and $|u_{113}(t)|_{\max}$. Among the four curves, the solid ones are for node 1 and the dashed ones are for node 38. From Figure 10(a) one sees that each curve has a peak when the pulsating frequency μ_e approaches the first un-damped natural frequency μ_1 of the pipe (i.e., $\mu_e \approx \mu_1 = 17.2773$ rad/s), this is because the both horizontal displacements are in the rightward $(+\bar{x})$ direction. However, from Figure 10(b) one sees that the solid curve for the vertical *downward* $(-\bar{y})$ displacements of node 1 has a peak at $\mu_e \approx \mu_1 = 17.2773$ rad/s, and the dashed curve for the vertical u*pward* $(+\bar{y})$ displacements of node 38 has a peak at $\mu_e \approx \mu_2 = 19.5136$ rad/s. It is seen that either horizontal or vertical displacement amplitudes, those of node 1 at the left free end of the pipe are much greater than the corresponding ones at the intermediate node 38. In addition, the maximum *vertical* displacement amplitude at node 1,

$|-u_2(t)|_{\max} \approx 0.125\text{m}$ shown in Figure 10(b) is much greater than the corresponding quasi-static deflection $|-\Delta_{1y}| \approx 0.021\text{m}$ shown in Figure 8(b) or 9(b). This result indicates that the S-pipe is safe under constant (quasi-static) loads and may be questionable under pulsating (dynamic) loads, particularly because it is deeply under the free water surface (with $h_{\max} = 35$ m).

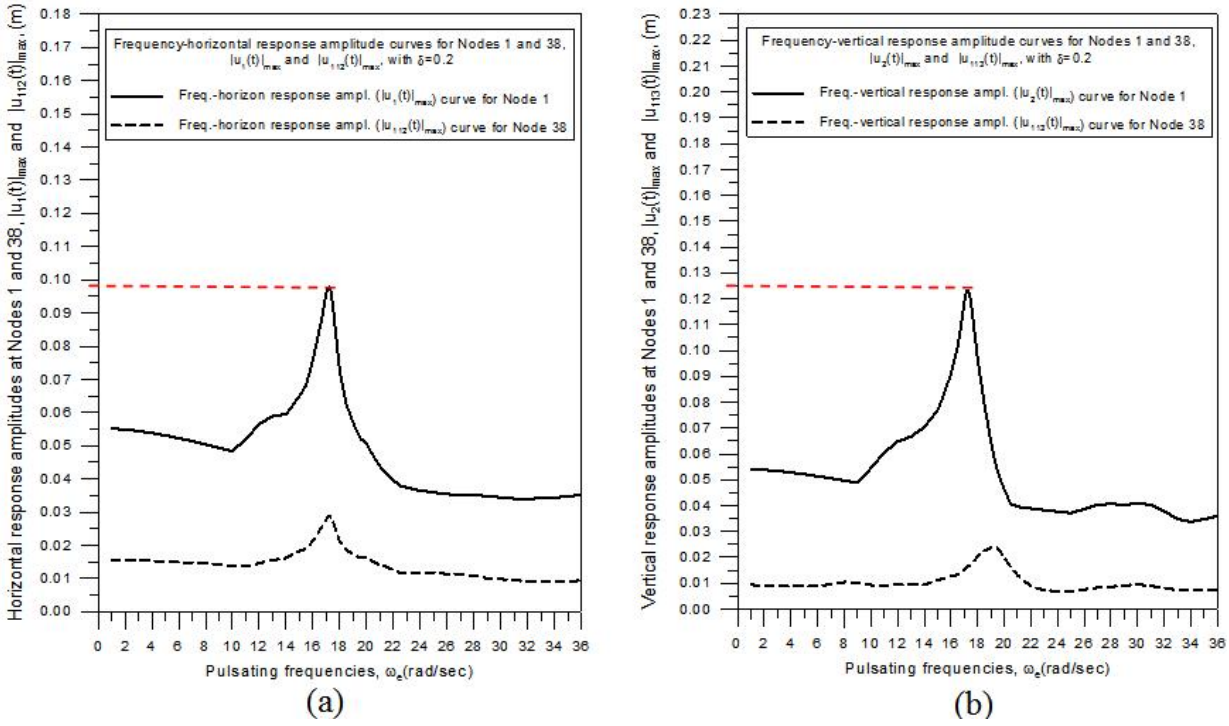

Figure10: For the Case of $¢ = 0.2$ and the Conditions given by Equation (27), the Frequency-Response Amplitude Curves for Nodes 1 and 38: (a) Horizontal ($\bar{x}$) Displacement Amplitudes, $|u_1(t)|_{\max}$ and $|u_{112}(t)|_{\max}$; (b) Vertical ($\bar{y}$) Displacement Amplitudes, $|-u_2(t)|_{\max}$ and $|u_{113}(t)|_{\max}$

If all conditions for Figure 10 are kept unchanged except that $¢ = 0.4$, then, the frequency-response amplitude curves for nodes 1 and 38 are shown in Figure 11(a) and (b), respectively. It is seen that, either the horizontal or vertical displacement amplitudes, the peak values shown in Figure 11(a) and (b) for the case of $¢ = 0.4$ are much greater than the corresponding ones shown in Figure 10(a) and (b) for the case of $¢ = 0.2$. This result is under our expectation, because $|V(t)|_{\max} = 1.2V_0$ if $¢ = 0.2$, and $|V(t)|_{\max} = 1.4V_0$ if $¢ = 0.4$, so that the ratio between the exciting force amplitudes for the last two cases is $|\bar{F}(t)|_{¢=0.4} / |\bar{F}(t)|_{¢=0.2} = (1.4V_0)^2/(1.2V_0)^2 \approx 1.361$. From Figure 11(b), one obtains the maximum *vertical* displacement amplitude at node 1, $|-u_2(t)|_{\max} \approx 0.227\text{m}$, which is 1.816 times the corresponding one $|-u_2(t)|_{\max} \approx 0.125\text{m}$ obtain from Figure 10(b) for the case of $¢ = 2.0$ and 10.81 times the quasi-static deflection $|-\Delta_{1y}| \approx 0.021\text{m}$ obtained from Figure 8(b) for the case of $¢ = 0$. It is noted that $0.227\text{m}/0.125\text{m} = 1.816$, this is greater than the exciting force amplitude ratio 1.361, due to the dynamic magnification effect. Such a nonlinear raise of dynamic response amplitudes of the S-pipe with the increase of pulsating parameter $¢$ may be the negative information for the safety of the S-pipe after the operation.

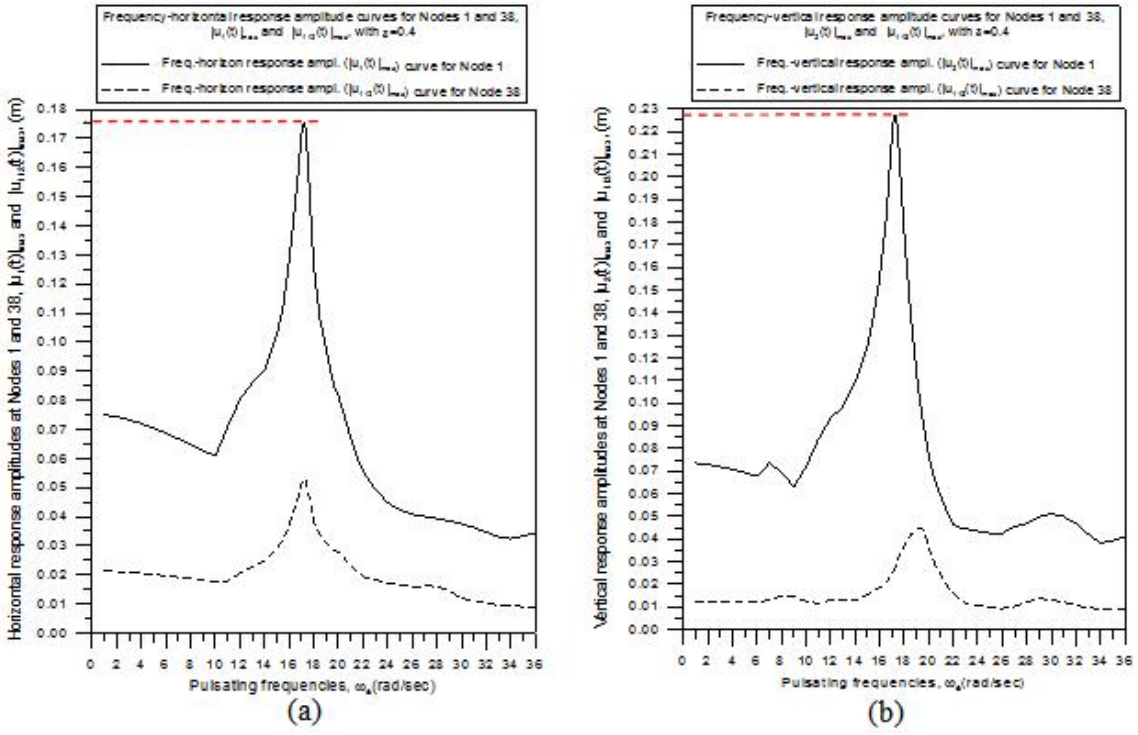

Figure 11: All Legends are the Same as Figure 10 Except that $\zeta = 0.4$ (Instead of $\zeta = 0.2$)

CONCLUSIONS

Based on the foregoing numerical results and discussions, one obtains the following conclusions:

- For the actual S-pipe studied in this paper, the influence of water-surface elevation of the reservoir on its lowest five natural frequencies is negligible, however, the variation of fluid mass density (due to sediments) influences its free vibration characteristics to some degree.
- Because the damping effect due to Coriolis force is negligible, either the "quasi-static" or the "dynamic" deflections of the actual S-pipe at its free end (inlet) will become very large if the structural damping effect in not considered. In such a case, introducing the Rayleigh damping matrix in terms of *damping ratios* (ζ_1 and ζ_2) of the entire vibrating system will be much better than using the inner and outer *damping coefficients* (c_i and c_o) of each components, because the determination of *damping ratios* is easier and more practical than that of *damping coefficients*.
- For the S-pipe studied in this paper, the flowing velocity of fluid will induce a pair of impulsive forces at its inlet and outlet, as well as a pair of centrifugal forces at its first and second curved pipe segments. The pair of impulsive forces are equal to each other in magnitudes, opposite in directions and not collinear, thus, they produce an unbalanced couple, and so do for the pair of centrifugal forces. For the fluid flow with "constant" velocity V_0, the quasi-static deflection at inlet (located at free end) is negligible, however, for the fluid flow with "pulsating" velocity $V(t) = V_0(1 + \zeta \cos \mu_e t)$ and the pulsating frequency μ_e approaching the first natural frequency μ_1 of the pipe, the maximum deflection at inlet may be more than ten times that of the quasi-static deflection (dependent on the magnitude of pulsating parameter ζ). In such situation, the safety of the S-pipe may be questionable.

Particular attention should be paid to the *liquefaction* of soil contacting with the S-pipe, because this may be the main reason leading to collapse of the S-pipe. It is evident that the general *straight* pipes do not have the foregoing problems.

- For the S-pipe studied in this paper, attentions must be paid to the operations of the gate at the pipe outlet. It is possible that one cannot open or close the gate due to its unusual size and the huge hydraulic pressure or impulsive force on it.
- From the view point of safety, efficiency or practicality, the "siphon" shown in Figure A1 (in *Appendix* of this paper) should be better than the actual S-pipe shown in Figure 1.

ACKNOWLEDGEMENTS

This work is supported by the Ministry of Science and Technology, Taiwan, Republic of China: Grant No. MOST 105-2221-E-006-067.

REFERENCES

1. ***Aldraihem, O. J.*** *(2007). Analysis of the dynamic stability of collar-stiffened pipes conveying fluid, Journal of Sound and Vibration, 300, 453-465.*
2. ***Arguelles, J. and Casanova, E.*** *(2015). Steady-state response of a piping system under harmonic excitations considering pipe-support friction with variable normal loads, Journal of Pressure Vessel Technology, 137, 051801-1~10.*
3. ***Ashley, H. and Haviland, G.*** *(1950) Bending vibrations of a pipe line containing flowing fluid, Journal of Applied Mechanics, Trans. ASME, 72, 229-232.*
4. ***Bathe, K. J.*** *(1982). Finite element procedures in engineering analysis, Prentice-Hall, New York.*
5. ***Benjamin, T. B.*** *(1961a). Dynamics of a system of articulated pipes conveying fluid, I: Theory, Proceedings of the Royal Society (London), 261(A), 457-486.*
6. ***Benjamin, T. B.*** *(1961b). Dynamics of a system of articulated pipes conveying fluid, II: Experiments, Proceedings of the Royal Society (London), 261(A), 487-499.*
7. ***Chen, S. S.*** *(1971). Dynamic stability of tube conveying fluid, Journal of Engineering Mechanics, ASCE, 97, 1469-1485.*
8. ***Chen, S. S.*** *(1972). Flow-induced in-plane instabilities of curved pipes, Nuclear Engineering and Design, 23, 29-38.*
9. ***Chen, S. S.*** *(1973) Out-of-plane vibration and stability of curved tubes conveying fluid, Journal of Applied Mechanics, 40, 362-368.*
10. ***Chen W. H. and Fan, C.N.*** *(1987). Stability analysis with lumped mass and friction effects in elastically supported pipes conveying fluid, Journal of Sound and Vibration, 119(3), 429-442.*
11. ***Djondjorov, P., Vassilev, V. and Dzhupanov, V.*** *(2001). Dynamic stability of fluid conveying cantilevered pipes on elastic foundations, Journal of Sound and Vibration, 247(3), 537-546.*

12. **Garbow, B. S.** *(1977). Matrix Eigensystem Routines-EISPACK Guide Extension, Springer-Verlag, Berlin.*

13. **Gregory, R. W. and Paidoussis, M. P.** *(1966a). Unstable oscillation of tubular cantilevers conveying fluid, I: Theory, Proceedings of the Royal Society (London), 293(A), 512-527.*

14. **Gregory, R. W. and Paidoussis, M. P.** *(1966b). Unstable oscillation of tubular cantilevers conveying fluid, I: Experiments, Proceedings of the Royal Society (London), 293(A), 528-542.*

15. **Housner, G. W.** *(1952). bending vibrations of a pipe line containing flowing fluid, Journal of Applied Mechanics, Trans. ASME, 74, 205-208.*

16. **Hsu, C. S.** *(1963). On the parametric excitation of a dynamic system having multiple degree-of-freedom, Journal of Applied Mechanics, 30(3), 367-372.*

17. **Ibrahim, R. A.** *(2010). Overview of Mechanics of Pipes Conveying Fluids-Part I: Fundamental Studies, Journal of Pressure Vessel Technology, Transactions of the ASME, 132, 034001-32.4.*

18. **Ibrahim, R. A.** *(2011). Mechanics of Pipes Conveying Fluids-Part II: Applications and Fluidelastic Problems, Journal of Pressure Vessel Technology, Transactions of the ASME, 133, 024001-30.*

19. **Kohli, A. K. and Nakra, B. C.** *(1984). Vibration analysis of straight and curved tubes conveying fluid by means of straight beam finite elements, Journal of Sound and Vibration, 93(2), 307-311.*

20. **Long, R. H.** *(1955). Experimental and theoretical study of transverse vibration of tube containing flowing fluid, Journal of Applied Mechanics, 22(1), 65-68.*

21. **Lottati, I. and Kornecki, A.** *(1986). The effect of an elastic foundation and of dissipative forces on the stability of fluid-conveying pipes, Journal of Sound and Vibration, 109, 327-338.*

22. **Meirovitch, L.** *(1967). Analytical Methods in Vibrations, Macmillan Company, London.*

23. **Noah, S. T. and Hopkins, G. R.** *(1980). Dynamic stability of elastically supported pipes conveying pulsating fluid, Journal of Sound and Vibration, 71(1), 103-116.*

24. **Paidoussis, M. P. and Issid, N. T.** *(1974). Dynamic stability of pipes conveying fluid, Journal of Sound and Vibration, 267-294.*

25. **Paidoussis, M. P. and Laithier, B. E.** *(1976). Dynamics of Timoshenko beams conveying fluid, Journal of Mechanical Engineering Science, 18(4), 210-220.*

26. **Paidoussis, M. P. and Sundararajan, N. T.** *(1975). Parametric and combination resonances of a pipe conveying pulsating fluid. Journal of Applied Mechanics, 42, 780-784.*

27. **Paidoussis, M.P. and Issid, N.T.** *(1976). Experiments on parametric resonance of pipes containing pulsatile flow. Journal of Applied Mechanics, 43, 198-202.*

28. **Pao, H. F.** *(1967). Fluid Mechanics, Charles E. Merrill Books Inc., Columbus, Ohio*

29. **Przemieniecki, J. S.** *(1985). Theory of matrix structural analysis, McGraw-Hill, New York.*

30. **Richart, F. E., Jr., Hall, J. R., Jr. and Woods, R. D.** *(1970). Vibrations of Soils and Foundations, Prentice-Hall,*

Englewood Cliffs, N.J.

31. ***Ryu, B. J., Ryu, S. U., Kim, G. H. and Yim, K. B.*** *(2004). Vibration and dynamic stability of pipes conveying fluid on elastic foundations, Int. J. Korea Society of Mechanical Engineering, 18(12), 2148-2157.*
32. ***Sreejith, B., Jayaraj, k., Ganesan, N., Padmanabhan, C., Chellapandi, P. and Selvaraj, P.*** *(2004). Finite element analysis of fluid-structure interaction in pipeline systems, Nuclear Engineering and Design, 227, 313-322.*
33. ***Timoshenko, S., Young, D. H. and Weaver, JR.*** *(1974). Vibration Problems in Engineering, 4th Ed., John Wiley & Sons, Inc.*
34. ***To, C. W. S. and Healy, J. W.*** *(1986). Further comment on "Vibration analysis of straight and curved tubes conveying fluid by means of straight beam finite elements", Journal of Sound and Vibration, 105(3), 513-514.*
35. ***Wu, J.S. and Chang, C.Y.*** *(June 1988). Structural simplification of a jack-up rig and its dynamic responses in regular waves, Journal of Ship Research, 32(2), 134-153.*
36. ***Wu, J.S. and Shih, P.Y.*** *(2000a). The dynamic behavior of a finite railway under the high-speed multiple moving forces by using finite element method, Communications in Numerical Methods in Engineering, 16, 851-866.*
37. ***Wu, J.S. and Shih, P.Y.*** *(2000b). Dynamic responses of railway and carriage under the high-speed moving loads, Journal of Sound and Vibration, 236(1), 61-87.*
38. ***Wu, J.S. and Shih, P.Y.*** *(2001). The dynamic analysis of a multi-span fluid-conveying pipe subjected to external load, Journal of Sound and Vibration, 239(2), 201-215.*
39. ***Wu, J.S. and Chiang, L.K.*** *(2003). Free vibration analysis of arches using curved bean elements, International Journal for Numerical Methods in Engineering, 58, 1907-1936.*
40. ***Wu, J.S. and Chiang, L.K.*** *(2004). A new approach for free vibration analysis of arches with effects of shear deformation and rotary inertia considered, Journal of Sound and Vibration, 277, 49-71.*
41. ***Wu, J.S. and Chen, C.T.*** *(2010). Wave-induced vibrations of an axial-loaded immersed Timoshenko beam carrying an eccentric tip mass with rotary inertia, Journal of Ship Research, 54(1), 15-33.*
42. ***Burlev M. Ya, Kharitonov V. D & Nikolaev N. S****, Using Electric Impulses for Dehydration Materials, International Journal of Electrical and Electronics Engineering (IJEEE), Volume 6, Issue 2, February-March 2017, pp. 11-16*
43. ***Wu, J.S.*** *(2013). Analytical and Numerical Methods for vibration Analyses, John Wiley & Sons, Singapore Pte. Ltd.*
44. ***Wu, J.S., Lo, S.C. and Chao, R.M.*** *(2015). Dynamic stability and free vibration of multi-span fluid-conveying pipes, Int. J. of Materials Engineering and Technology, 14(1), 1-43.*
45. ***Yu, D., Paidoussis, M.P., Shen, H. and Wang, L.*** *(2014). Dynamic Stability of Periodic pipes conveying fluid, Journal of Applied Mechanics, 81, 011008-1~8.*

APPENDIX: CLEANING DEPOSIT OF TSEN-WENG RESERVOIR BY USING SIPHON

For leaning the deposit of Tsen-Weng reservoir, instead of the conventional sluice gate near free water surface, the siphon with its inlet near reservoir bottom (Figure A1) will be safer, more efficient and more practical.

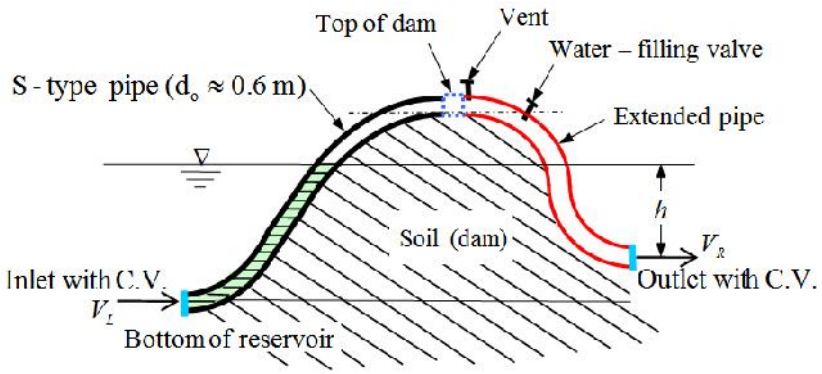

Figure A1: The Original Conception for Cleaning Deposit of Tsen-Weng Reservoir by Using Siphon Theory (C.V. = Control Valve)